

## Article

# Bimetallic Flower-like NiCoP Encapsulated in an N-Doped Carbon Shell with Enhanced Lithium Storage Properties

Haoyu Tian <sup>1,2,†</sup>, Lingyu Zhao <sup>2,3,†</sup>, Linlin Wang <sup>2,\*</sup>, Zijie Xia <sup>1,2</sup>, Wenqi Tan <sup>2</sup> and Zheng Jiao <sup>4,\*</sup>

<sup>1</sup> School of Environmental and Chemical Engineering, Shanghai University, 99 Shangda Road, Shanghai 200444, China; tianhaoyu@shu.edu.cn (H.T.)

<sup>2</sup> Institute for Sustainable Energy, College of Science, Shanghai University, Shanghai 200444, China; lingyuzhao@sues.edu.cn (L.Z.)

<sup>3</sup> College of Chemistry and Chemical Engineering, Shanghai University of Engineering Science, 333 Longteng Road, Shanghai 201620, China

<sup>4</sup> Applied Radiation Institute, Shanghai University, Shanghai 201800, China

\* Correspondence: wl.linlin@mail.ustc.edu.cn (L.W.); zjiao@shu.edu.cn (Z.J.)

† These authors contributed equally to this work.

**Abstract:** It continues to be a challenge to design innovative NiCoP composite anode materials to further improve rate capacity. In this work, bimetallic flower-like NiCoP encapsulated in an N-doped carbon shell (designated as NiCoP@NC) as a high-rate capable anode material for lithium-ion batteries (LIBs) was successfully designed and synthesized. The novel structure design combines the advantages of flower-like NiCoP (core) and N-doped carbon (shell). Flower-like NiCoP offers numerous interface and redox reaction sites for improving lithium storage, while the N-doped carbon shell effectively buffers volume expansion and enhances electrical conductivity. The synergistic effect between NiCoP and the N-doped carbon shell proposes a marvelous high-rate capacity (320 mA h/g even at 5 A/g) and a good cycle life with high reversible capacity (369.8 mA h/g for 700 cycles at 3 A/g with 81% retention). An investigation of kinetics performance shows that the introduction of the N-doped carbon shell enhances the charge transfer, and the pseudocapacitive behavior dominates the rapid Li<sup>+</sup> storage of the NiCoP@NC electrode.



**Citation:** Tian, H.; Zhao, L.; Wang, L.; Xia, Z.; Tan, W.; Jiao, Z. Bimetallic Flower-like NiCoP Encapsulated in an N-Doped Carbon Shell with Enhanced Lithium Storage Properties. *Batteries* **2023**, *9*, 361. <https://doi.org/10.3390/batteries9070361>

Academic Editors: Shen Wang, Jianbin Zhou and Carlos Zieberst

Received: 26 May 2023

Revised: 17 June 2023

Accepted: 23 June 2023

Published: 5 July 2023



**Copyright:** © 2023 by the authors. Licensee MDPI, Basel, Switzerland. This article is an open access article distributed under the terms and conditions of the Creative Commons Attribution (CC BY) license (<https://creativecommons.org/licenses/by/4.0/>).

## 1. Introduction

To meet the growing need for increased energy consumption, secondary batteries are gaining more significance in energy storage. Lithium-ion batteries (LIBs) are widely applied for energy storage in electric vehicles, digital communications, and mobile electronic devices because of their high energy density and rechargeable capabilities [1–5]. However, traditional LIBs are unable to fulfill the fast-paced expansion of demand. Graphitic carbon, as a traditional anode material, is extensively applied for LIBs in commerce. The energy density of LIBs is severely restricted because of their low theoretical specific capacity of only 372 mA h/g. Thus, developing anode materials possessing higher theoretical specific capacities and stability of cycling is essential for improving the electrochemical performance of LIBs.

Transition metal compounds, especially transition metal phosphides (TMPs) and transition metal organic frameworks (MOFs), are promising materials applied in the fields of energy storage and as electrocatalysts due to their high thermal stability and low cost [6–8]. Compared to traditional intercalation carbon materials, TMPs possess much higher theoretical specific capacities due to the conversion reaction ( $M_{\text{P}}_x + 3 \times \text{Li} \rightarrow x \text{Li}_3\text{P} + M$ ), offering more Li exchanged per formula unit. In addition, TMPs exhibit the lowest lithiation potential in comparison with transition metal oxides and transition metal sulfides, which contributes to the highest theoretical capacity and reduces the formation of lithium metal dendrites [9]. Therefore, TMPs as anode materials have emerged as highly competitive candidates for

LIBs. Nonetheless, limited electrical conductivity and severe volume expansion during repeated  $\text{Li}^+$  insertion/extraction leads to capacity fading and poor cycling stability, limiting their practical applications in high-performance LIBs [10–12].

Among these TMPs, bimetallic NiCoP has received gradually growing interest as electrocatalyst material for water splitting and supercapacitors in recent years [13,14]. However, compared to the aforementioned applications, NiCoP as an anode material for LIBs has received less attention in research and development [15,16]. NiCoP, as an anode material for LIBs, demonstrates low lithiation voltage and high specific capacity, presenting higher electrochemical performance than the monometals  $\text{CoP}_x$  and  $\text{NiP}_x$ . The presence of Ni and Co species in NiCoP can easily form an alloy because they possess similar physical and chemical characteristics, leading to higher specific capacity and structural stability, while the Co species contributes to structural stability, and the Ni species contributes to high specific capacity [17,18]. Due to the above potential characteristics, NiCoP has emerged as a highly promising candidate as an anode material for LIBs. However, it also suffers from capacity diminishing, especially at high rates, because of the large volume expansion during  $\text{Li}^+$  insertion/extraction and limited electrical conductivity [19].

Designing the nanostructure of materials and combining them with different types of carbon materials, including carbon nanofibers [20], carbon nanotubes [21], graphene [22], and amorphous carbon [23], has proven to be a highly effective method for addressing limited electrical conductivity and severe volume expansion during cycling. For instance, Wang et al. synthesized bimetal phosphide nanoparticles with a carbon shell ( $\text{Ni}_{1.4}\text{Co}_{0.6}\text{P/C}$ ) embedded into a nitrogen-doped graphene (NGN) base using a solution-phase self-assembly strategy [16].  $\text{Ni}_{1.4}\text{Co}_{0.6}\text{P/C@NGN}$  exhibits favorable rate capacities of 502 mA h/g and 227 mA h/g at 0.12 A/g and 3 A/g and then back to 444 mA h/g at 0.12 A/g, with a capacity retention ratio of 74%, as an anode material for LIBs.  $\text{Ni}_{1.4}\text{Co}_{0.6}\text{P/C@NGN}$  not only offers a large number of active sites for loading NiCoP nanoparticles, but it also capably buffers large volume expansion and boosts electrical conductivity. Li et al. synthesized NiCoP microsphere architecture through a hard-template method [24]. Since the morphology of micron-size spheres encapsulated in needle-like nanowires provides numerous active sites and structural stability for lithium storage, microsphere NiCoP electrodes exhibit excellent high rate capacities of 190 mA h/g, 137 mA h/g, and 78 mA h/g at 1 A/g, 2 A/g, and 3 A/g, respectively. Wang et al. prepared a composite comprising NiCoP and carbon nanotubes (NiCoP/CNTs) using a one-pot method [25]. The results show rate capacities of 118 mA h/g and 88 mA h/g at 0.1 A/g and 1 A/g and then back to 118 mA h/g at 0.1 A/g as anode materials for LIBs. The improved electrochemical performance of NiCoP/CNTs can be attributed to the interface between NiCoP and CNTs for increasing electrical conductivity. Wang et al. developed graphene-supported NiCoP nanoparticles using a solution-phase self-assembly strategy with a high rate capacity of 74 mA h/g at even 5 A/g and 532 mA h/g at 0.1 A/g after 100 cycles, with 78.2% capacity retention [26]. Even though rate performance has been enhanced by using carbon composites with various nanostructures to decorate the NiCoP, developing an innovative NiCoP composite structure to further promote rate capacities at high rates is still a challenging task.

In this work, flower-like NiCoP encapsulated in an N-doped carbon shell (NiCoP@NC) was successfully designed and synthesized. Flower-like NiCoP offers numerous redox reaction sites for lithium storage, while the N-doped carbon shell effectively buffers volume expansion and enhances electrical conductivity. Benefiting from the novel structural design, NiCoP@NC shows a high rate capability (320.0 mA h/g at 5 A/g), high specific capacity (545.3 mA h/g at 0.1 A/g, with 89% retention), and long-term cycling capacity (369.8 mA h/g after 700 cycles at 3 A/g, with 81% retention) for LIBs.

## 2. Materials and Methods

### 2.1. Materials for Synthesis

All chemical reagents were purchased from Shanghai Aladdin Biochemical Technology Co., Ltd., China, including nickel nitrate hexahydrate ( $\text{Ni}(\text{NO}_3)_2 \bullet 6\text{H}_2\text{O}$ , purity  $\geq 99.0\%$ ),

cobalt nitrate hexahydrate ( $\text{Co}(\text{NO}_3)_2 \bullet 6\text{H}_2\text{O}$ , purity  $\geq 99.0\%$ ), hexamethylene tetramine ( $\text{C}_6\text{H}_{12}\text{N}_4$ , purity  $\geq 99\%$ ), absolute ethanol ( $\text{C}_2\text{H}_5\text{OH}$ , purity  $\geq 99\%$ ), dopamine hydrochloride ( $\text{C}_8\text{H}_{12}\text{ClNO}_2$ , purity  $\geq 99\%$ ), sodium hypophosphite ( $\text{NaH}_2\text{PO}_2$ , purity  $\geq 99\%$ ), tris(hydroxymethyl)aminoethane ( $\text{C}_4\text{H}_{11}\text{NO}_3$ , purity  $\geq 99\%$ ), and hydrochloric acid (HCl, purity  $\geq 99\%$ ), without any purification.

## 2.2. *NiCoP@NC Synthesizing*

First, in a typical synthesizing process, 1 mmol  $\text{Co}(\text{NO}_3)_2 \bullet 6\text{H}_2\text{O}$ , 2 mmol  $\text{Ni}(\text{NO}_3)_2 \bullet 6\text{H}_2\text{O}$ , and 6 mmol hexamethylene tetramine ( $\text{C}_6\text{H}_{12}\text{N}_4$ ) were dispersed in a mixture of solvent that included 20 mL absolute ethanol and 40 mL deionized water. It was stirred continuously for 1 h until a pink transparent solution formed. The pink mixture was poured into a 100 mL polytetrafluoroethylene lined stainless autoclave and kept at 100 °C for 10 h. After cooling to room temperature, the green precipitate NiCo-OH precursor was obtained via centrifugation, washed several times with deionized water and absolute ethanol, and dried under vacuum at 60 °C for 12 h. Second, the as-prepared NiCo-OH (100 mg) was distributed in a Tris-HCl buffer mixed solution (50 mL, 2.5 mM, pH = 8.5) with magnetic stirring for 30 min, and dopamine hydrochloride (25 mg) was dispersed and blended continuously for 12 h until forming a polydopamine (PDA) shell and adhering to the surface of the NiCo-OH. The brown precipitate denoted as NiCo-OH@PDA was obtained via centrifugation, washed several times with deionized water and absolute ethanol, and dried under vacuum at 60 °C for 12 h. Third, the prepared NiCo-OH@PDA (100 mg) and  $\text{NaH}_2\text{PO}_2$  (1 g) were placed in a porcelain boat. To synthesize NiCoP@NC,  $\text{NaH}_2\text{PO}_2$  was used as the source of phosphorus, and a tube furnace was positioned upstream. The NiCo-OH@PDA and  $\text{NaH}_2\text{PO}_2$  were heated at 400 °C for 2 h at a rate of 1 °C/min under an Ar atmosphere to acquire the target product, black powder NiCoP@NC. For comparison, bare NiCoP was obtained through the phosphorization of NiCo-OH.

## 2.3. *Material Characterizations*

The surface morphology and structure of the NiCoP@NC sample were observed and characterized using a scanning electron microscope (SEM) (JEM-7610CX, JEOL, Tokyo, Japan). Further characterization of the morphology and structure of NiCoP@NC was conducted using transmission electron microscopy (TEM) (200CX, JEOL). The crystal features were characterized using HRTEM. The crystal phases of the NiCoP@NC and NiCoP were analyzed using X-ray diffraction (XRD) with Cu K $\alpha$  radiation ( $k = 1.5418 \text{ \AA}$ ) on a D8-advance (Bruker, Karlsruhe, Germany) to investigate the crystal structure. X-ray photoelectron spectroscopy (XPS) characterized NiCoP@NC using a Thermo ESCALAB 250XI (Thermo Fisher Scientific, Waltham, MA, USA) with an Al K $\alpha$  light source. The binding energy data were rectified via the peak at 284.8 eV corresponding to C 1s.

## 2.4. *Electrochemical Analyses*

To fabricate a working electrode, the mixture (active materials: carbon black: 5% polyvinylidene fluoride (PVDF) binder = 7:2:1, weight ratio) was ground for 30 min to form an evenly dispersed electrode slurry. The prepared electrode slurry was spread evenly onto copper foil. The copper foil with the electrode slurry was then moved into a vacuum oven to dry at 100 °C for 12 h. Each electrode piece possessed approximately 1.2 mg of active materials. CR2016 button cells were assembled inside a glove box (Mikrouna Super 1220, Shanghai, China) operating under a full Ar atmosphere. Lithium metal foil was utilized as the reference electrode and counter electrode. A micropore polypropylene membrane (Celgard 2600, Celgard LLC, Charlotte, NC, USA) was employed as the separator. The electrolytes included 1.0 M  $\text{LiPF}_6$ , ethylene carbonate (EC)/diethyl carbonate (DEC) (1:1 volume ratio), and 5.0% fluoroethylene carbonate (FEC). An Autolab electrochemical workstation (PGSTAT302N, Metrohm, Shanghai, China) was used for evaluating cyclic voltammetry (CV) curves at various scan rates in the potential from 0.01 to 3.0 V, and electrochemical impedance spectroscopy (EIS) was used in the frequency from 0.01 Hz to

100 kHz. Cycling and rating performances between 0.01 V and 3.0 V were carried out on a LAND (CT2001A, LANHE, Wuhan, China).

### 3. Results and Discussion

#### 3.1. Morphology and Structure

Figure 1a demonstrates the routine for synthesizing NiCoP@NC. First, a hydrothermal reaction was performed to synthesize a flower-like NiCo-OH green precipitate. Then, the NiCo-OH was coated with dopamine, forming NiCo-OH@PDA as a brown precipitate. The dopamine molecule was oxidized and polymerized in Tris-HCl buffer to obtain polydopamine. During polymerization, polydopamine closely adhered on the surface of NiCo-OH via  $\pi-\pi^*$  bonding interactions [27]. Finally, the flower-like NiCoP encapsulated in the N-doped carbon shell (NiCoP@NC) was converted from NiCo-OH@PDA via annealing with  $\text{NaH}_2\text{PO}_2$  under an Ar atmosphere involving phosphorization of the NiCo-OH processes and carbonization of the N-doped carbon shell processes, simultaneously. Figure 1b–d show the low magnification SEM images of NiCo-OH and NiCoP@NC. It can be perceived that the morphology of the NiCo-OH precursor is multiple and uniform micron-sized flowers consisting of numerous thin flakes. The high magnification SEM images of NiCo-OH and NiCoP@NC are shown in Figure 1c,e. The NiCoP@NC maintains the morphology and structure of the NiCo-OH precursor and shows similar flowers with a diameter of approximately 3  $\mu\text{m}$ , but thin flakes of the flower grow significantly thicker due to coating via the N-doped carbon shell. The flower-like structure of NiCoP@NC as an anode material could provide endurance for repeated  $\text{Li}^+$  insertion/extraction processes and numerous redox reaction sites, while the N-doped carbon shell effectively buffers the volume expansion. The synergistic effect results in the enhancement of the electrochemical performance of LIBs [20].

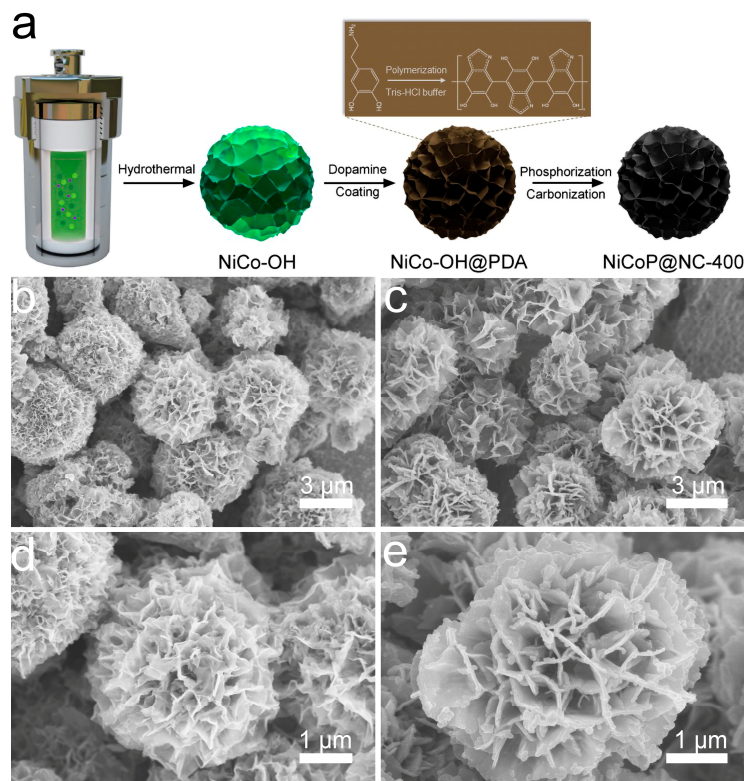


**Figure 1.** (a) Synthesis of NiCoP@NC; (b–e) Different magnification SEM images of precursor NiCo-OH and NiCoP@NC.

Figure 2 presents different magnifications of TEM and element mapping images of NiCoP@NC. In Figure 2a, the single flower-like NiCoP (core) encapsulated in the N-doped

carbon (shell) can be perceived. As presented in Figure 2b,c, the TEM images at high magnifications further exhibit the interface between the thin flakes of the flower-like NiCoP and the coating N-doped carbon shell. An HRTEM image of the NiCoP@NC (Figure 2d) demonstrates that the marked lattice fringe d-spacing is 0.21 nm and can be assigned to (111) planes of the NiCoP phase. An HAADF-STEM image and elemental mappings for NiCoP@NC in Figure 2e show C, N, Ni, Co, and P elements that are homogeneously dispersed throughout the structure. This confirms that we successfully synthesized NiCoP@NC.

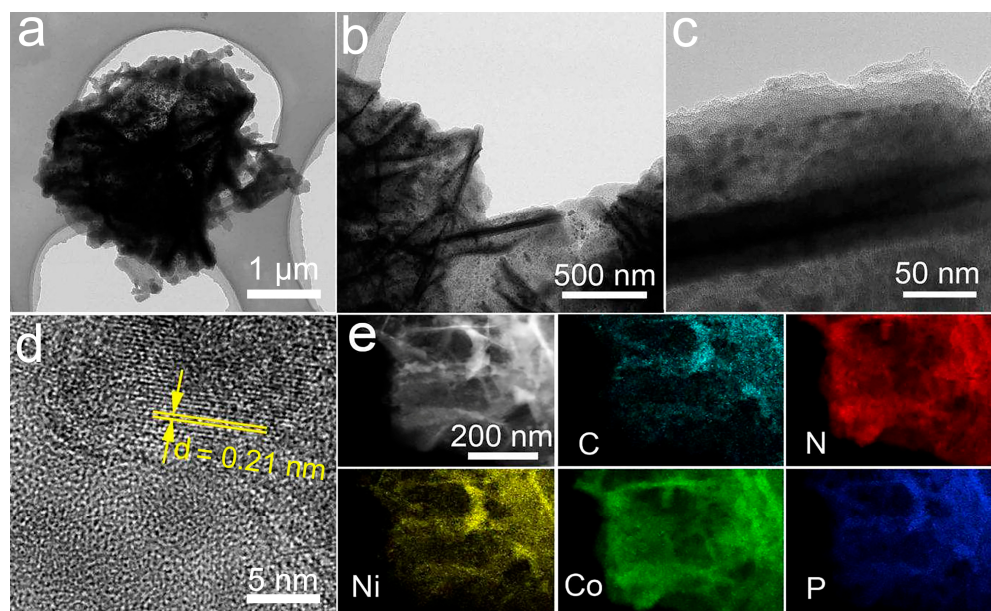


**Figure 2.** (a–c) Different magnification TEM images of NiCoP@NC; (d) an HRTEM lattice image of NiCoP@NC; (e) HAADF-STEM and elemental mapping images of NiCoP@NC, including C, N, Ni, Co, and P.

XRD patterns were measured for characterizations of NiCoP@NC and NiCoP compositions. Figure 3a shows several distinct diffraction peaks appearing at  $41.10^\circ$ ,  $44.91^\circ$ ,  $47.61^\circ$ ,  $54.41^\circ$ , and  $55.31^\circ$ , which are, respectively, attributed to the (111), (201), (210), and (002) planes of NiCoP (JCPDS No: 71-2336), while the bulging peak after  $20^\circ$  indicates the presence of amorphous carbon [28]. The XRD of NiCoP is similar to that of Ni<sub>2</sub>P (JCPDS No: 89-2742), indicating that Ni<sub>2</sub>P and NiCoP share the same crystal structure. By contrast, the XRD pattern of NiCoP is significantly different from that of CoP (JCPDS No: 29-0497). In addition, the pattern of NiCoP@NC does not exhibit any of the distinct diffraction peaks of CoP. The evidence suggests that Co atoms are successfully introduced into the Ni<sub>2</sub>P crystal lattice and maintain its crystal structure instead of a combined CoP and Ni<sub>2</sub>P composition. The chemical formula and valence state in oxidation of the NiCoP@NC surface were investigated using XPS. In Figure 3b, the XPS spectrum demonstrates that P, C, N, O, Ni, and Co elements exist on the NiCoP@NC surface, fitting well with the results of the elemental mapping. The C 1s high-resolution spectrum is made up of four distinct segments. Specifically, the binding energies of 284.6 eV, 285.1 eV, 285.7 eV, and 286.7 eV correspond to C–C, C–P, C–N, and O=C–O, respectively (Figure 3c) [29]. The N 1s spectrum, as depicted in Figure 3d, reveals the presence of pyridinic-N (399.9 eV), pyrrolic-N (401.5 eV), and graphitic-N (402.3 eV) in the N 1s region. The C 1s and N 1s XPS spectra suggest that the N element was successfully introduced into the carbon lattice, which is identical to the XRD results. The N species efficiently boosted the electrical conductivity of the carbon by offering electrons; however, its properties are very different from each other. Pyridinic-N and pyrrolic-N strengthen electrochemical performance, while graphitic-N only causes poor cycling stability and electrochemical performance. Pyridinic-N and

pyrrolic-N in carbon offer abundant defects and active sites for electrochemical reactions, which promote the stabilization of ions by electro-adsorption on the carbon interface. In contrast, graphitic-N reacts with  $\text{Li}^+$  irreversibly, which leads to irreversibility of capacity and a decrease in electrochemical performance. Graphitic-N would be formed by the conversion of pyridinic-N and pyrrolic-N in carbonization and could only be removed by denitrification [30]. Figure 3e shows that the spectrum of Ni 2p is fragmented for three spin-orbit double peaks and accords to the  $\text{Ni}^{2+}$  characteristic peaks. The characteristic peak of Ni in Ni 2p can be observed at 853.4 eV. The Ni 2p<sub>3/2</sub> and Ni 2p<sub>1/2</sub> centered on 853.4 eV and 874.4 eV are both +2 valence states of Ni. Moreover, the peaks centered on 861.7 eV and 880.3 eV can be attributed to corresponding with the Ni 2p<sub>3/2</sub> and Ni 2p<sub>1/2</sub> subsequent peaks, respectively. Figure 3f demonstrates the XPS spectrum of Co 2p, which exhibits three pairs of double peaks in the  $\text{Co}^{2+}$  state. The Co characteristic peak is observed at 778.6 eV, while Co 2p<sub>3/2</sub> and Co 2p<sub>1/2</sub> are the characteristic peaks perceived at 793.5 eV and 797.8 eV, respectively. Figure 3g depicts the P 2p spectrum of NiCoP@NC, which consists of three peaks. The binding energy is perceived at 129.5 eV and 130.3 eV relating to P 2p<sub>3/2</sub> and P 2p<sub>1/2</sub>, which are ascribed to the presence of the P species. Moreover, the peak positioned at 133.5 eV represents the P–O bond [31,32]. The above XRD and XPS results demonstrate that NiCoP@NC was successfully synthesized.

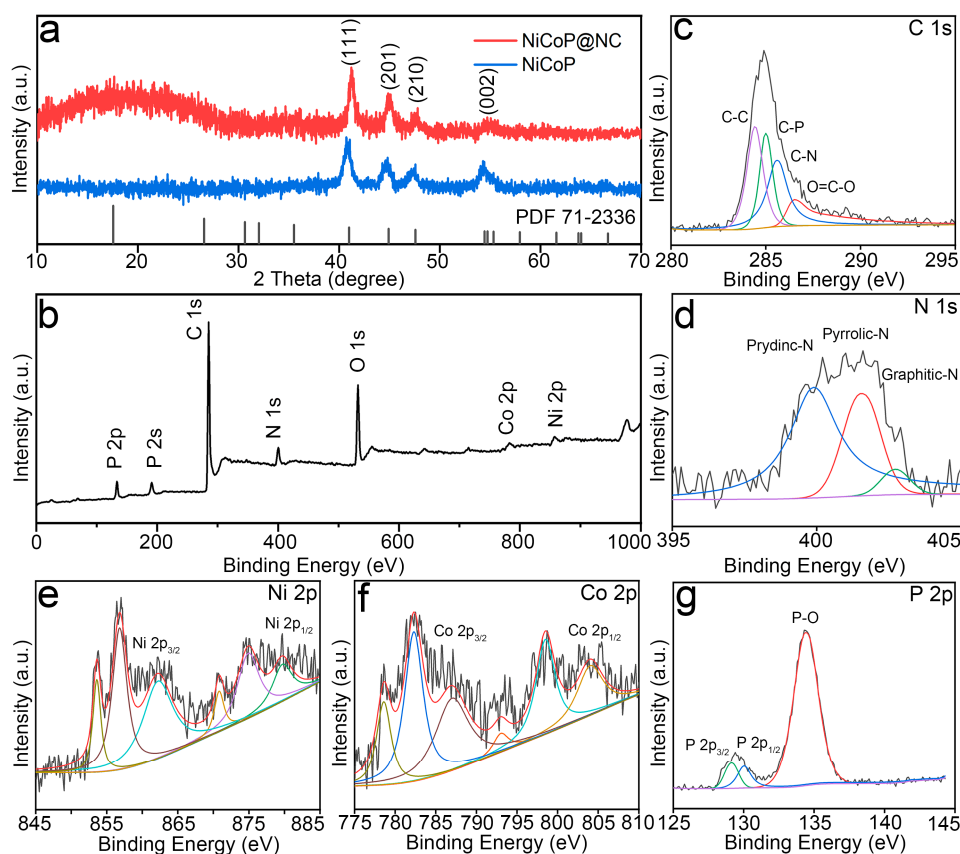


**Figure 3.** XRD patterns of (a) NiCoP@NC and NiCoP; XPS spectra of NiCoP@NC; (b) survey spectrum; (c–g) C 1s, N 1s, Ni 2p, Co 2p, and P 2p, respectively.

### 3.2. Electrochemical Performance

To investigate electrochemical behavior in detail, cyclic voltammogram (CV) curves of the electrodes were measured during  $\text{Li}^+$  insertion/extraction in the voltage range 0.01–3 V at a scan rate of  $0.1 \text{ mV s}^{-1}$  versus  $\text{Li}^+/\text{Li}$ . The first five CV curves of the NiCoP@NC electrode are displayed in Figure 4. In the first discharge, a reduction peak at 1.6 V corresponds to the formation of the metals Co and Ni and the amorphous  $\text{Li}_3\text{P}$

transformation reaction, while another reduction peak located 0.8 V may correspond to the simultaneous formation of  $\text{Li}_3\text{P}$  and SEI films. During the charging process, the oxidation peaks at ~1 V and ~1.3 V are related to the decomposition of  $\text{Li}_3\text{P}$ . After the initial cycle, the main peaks at the cathode become ~1.72 V and ~1.8 V due to the redox reaction between  $\text{Li}_3\text{P}$  and  $\text{LiP}$ , respectively, and the cathode peaks below 0.8 V disappear, indicating the stability of the SEI film. The CV curves from the second to the fifth overlap well, indicating the excellent stability of the anode materials during cycling.

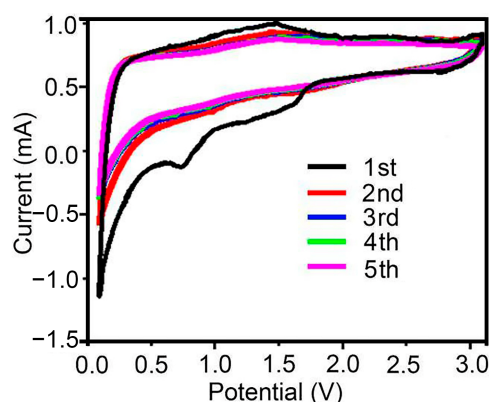


**Figure 4.** Electrochemical measurements of the NiCoP@NC, CV curves of the NiCoP@NC electrode for the first to fifth cycles at  $0.1 \text{ mV s}^{-1}$ .

The NiCoP@NC and NiCoP electrodes were tested for LIBs to investigate their electrochemical properties. We compared the cycling performance of the NiCoP@NC and NiCoP electrodes at  $0.1 \text{ A/g}$  and  $1 \text{ A/g}$ , respectively. The cycling performances of the bare NiCoP and NiCoP@NC electrodes at  $0.1 \text{ A/g}$  are exhibited in Figure 5a. The initial discharge/charge capacity of bare NiCoP is  $312.17/180.84 \text{ mA h/g}$ , with an initial columbic efficiency (ICE) of 57.7%, while that of NiCoP@NC is  $1025.12/628.19 \text{ mA h/g}$ , with an ICE of 61.2%, exhibiting a significant increase in ICE. The loss of irreversible capacity in the initial cycle is primarily attributed to forming a solid electrolyte interface (SEI) layer on the active material surface. For 100 cycles, the reversible capacity of the NiCoP@NC electrode is approximately  $545.3 \text{ mA h/g}$ , with a capacity retention ratio of 89%, while the capacity of the bare NiCoP electrode is fading rapidly, maintaining  $185.8 \text{ mA h/g}$ , with a capacity retention ratio of 45%. During the charge/discharge process, the impairment of the structure leads to the rapid fading of capacity. As perceived in Figure 5b, it exhibits the cycling properties of NiCoP@NC and NiCoP; they maintain discharge capacities of  $537.0 \text{ mA h/g}$  and  $78.0 \text{ mA h/g}$  for 100 cycles at  $1 \text{ A/g}$ , with capacity retention ratios of 90% and 76%, respectively. The specific capacity and cycling stability of the NiCoP@NC electrode are considerably higher compared to the NiCoP electrode. The synergistic effect between NiCoP and the N-doped carbon shell results in marvelous capacity retention. Figure 5c exhibits that the rate performances of the NiCoP@NC electrode at  $0.1, 0.2, 0.5, 1, 2$ , and  $5 \text{ A/g}$  are  $680.3, 540.8, 487.7, 400.7, 368.4$ , and  $320.0 \text{ mA h/g}$  respectively. The discharge capacity ascends to  $653.4 \text{ mA h/g}$  due to backs to  $0.1 \text{ A/g}$ , with a capacity retention ratio of 96%. As for the NiCoP electrode, its rate performances at the same current densities are  $394.6, 292.6, 193.6, 150.7, 136.4$ , and  $94.0 \text{ mA h/g}$ , and it rises again to  $320.2 \text{ mA h/g}$  at  $0.1 \text{ A/g}$ , with a capacity retention ratio of 81%. When coating with the N-doped carbon, the rate capacity of the NiCoP@NC electrode is significantly improved in comparison with the bare NiCoP electrode. The N-doped carbon shell not only enhances the electrical conductivity but also plays a role in the volume expansion buffer. Compared to other previously reported NiCoP composite anode materials for LIBs [16,24–26], NiCoP@NC still shows a superior rate performance, which is depicted in Figure 5d. The cycling stability of NiCoP@NC with rapid lithium storage performance was further investigated using long-term cycling at a high current density of up to  $3 \text{ A/g}$ . The NiCoP@NC electrode

still maintains a high reversible discharge capacity of 369.8 mA h/g, even after 700 cycles, with a good capacity retention ratio of 81% beginning at the third cycle (Figure 5e). The above results display that flower-like NiCoP@NC delivers outstanding rate capacity and long-term stable cycling properties.

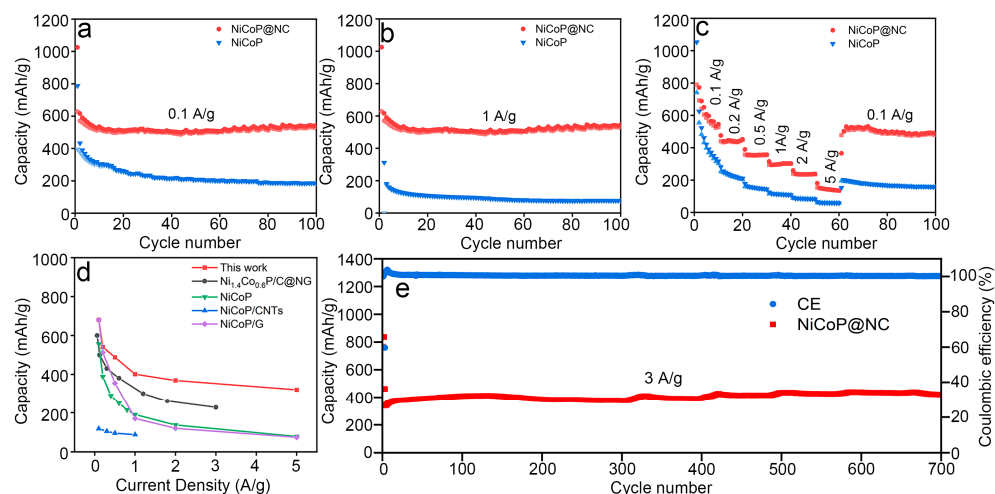


**Figure 5.** (a,b) At current densities of 0.1 A/g and 1 A/g, the cycling performances of NiCoP@NC and bare NiCoP, respectively; (c) Rate performance of NiCoP@NC and bare NiCoP; (d) Comparison with reported NiCoP composite anode materials for LIBs; (e) Long-term and high current density cycling performance of NiCoP@NC.

The superior kinetic performance of NiCoP@NC was studied using EIS measurements of the NiCoP@NC and bare NiCoP electrodes to investigate the outstanding electrochemical performance of the NiCoP@NC electrode (Figure 6a). A Nyquist diagram of the two samples shows an impedance spectrum consisting of the region in high frequency as shapes of semicircles and the region in low frequency as shapes of inclined straight lines. At the electrolyte/electrode interface, the solution resistance ( $R_1$ ) and charge transfer impedance ( $R_2$ ) are correlated with the diameters of the semicircles, while the slope corresponds to the Warburg impedance ( $R_W$ ), indicating the  $\text{Li}^+$  diffusion coefficient. The NiCoP@NC electrode demonstrates lower solution resistance and charge transfer resistance ( $R_1 = 4.67 \Omega$ ,  $R_2 = 54.32 \Omega$ ) than NiCoP ( $R_1 = 8.82 \Omega$ ,  $R_2 = 119.7 \Omega$ ). The consequence shows that the N-doped carbon shell considerably enhances electrical conductivity and ion diffusion efficiency, further demonstrating the favorable influence of the N-doped carbon shell coated on NiCoP [33–35]. The NiCoP@NC demonstrates superior electrochemical performance due to its reduced charge transfer resistance. These advantages particularly benefit its rate capacity, allowing for rapid lithium storage. To comprehensively investigate the NiCoP@NC reaction kinetics, CV curves were measured using various scan rates (0.2–1.0 mV/s) (Figure 6b). Universally, the peak current and scan rate are related by the subsequent formulas:

$$i = a v^b \quad (1)$$

$$\log i = \log a + b \log v \quad (2)$$

where  $i$ ,  $v$ ,  $a$ , and  $b$  represent peak current, scanning rate, and constant parameters, respectively. The  $b$ -value, which is the calculated slope from Formulas (1) and (2), ranges from 0.5 to 1, and it evaluates the electrochemical behavior, indicating the contributions of capacitive- and diffusion-controlled processes. The diffusion-controlled process of the  $b$ -value is approximately 0.5, while the capacitive-controlled process of the  $b$ -value is approximately 1. Figure 6c demonstrates that the  $b$ -value of the anode/cathode peak of the NiCoP@NC electrode is obtained at 0.789/0.967, indicating that the electrodes exhibit a jointly controlled reaction kinetic process that includes capacitive-and diffusion-controlled behaviors.

Furthermore, by analyzing the CV curves, the capacitive- and diffusion-controlled contributions are evaluated using the following formula:

$$i = k_1 v + k_2 v^{1/2} \quad (3)$$

In Figure 6d, the NiCoP@NC electrode's capacitive contribution rate is calculated to be 74.8% at 0.8 mV/s, based on Formula (3). In addition, Figure 6e shows that the distribution of the capacitive contribution is ascending and that the scan rate is escalating from 0.2 mV/s to 1 mV/s. The distributions of the capacitive contribution are 60.0%, 62.2%, 63.4%, 74.8%, and 75.8% at scan rates of 0.2, 0.4, 0.6, 0.8, and 1.0 mV/s, respectively. The ascending capacitive contribution ratio of NiCoP@NC significantly influences the reaction kinetics, boosting the NiCoP@NC electrochemical properties.

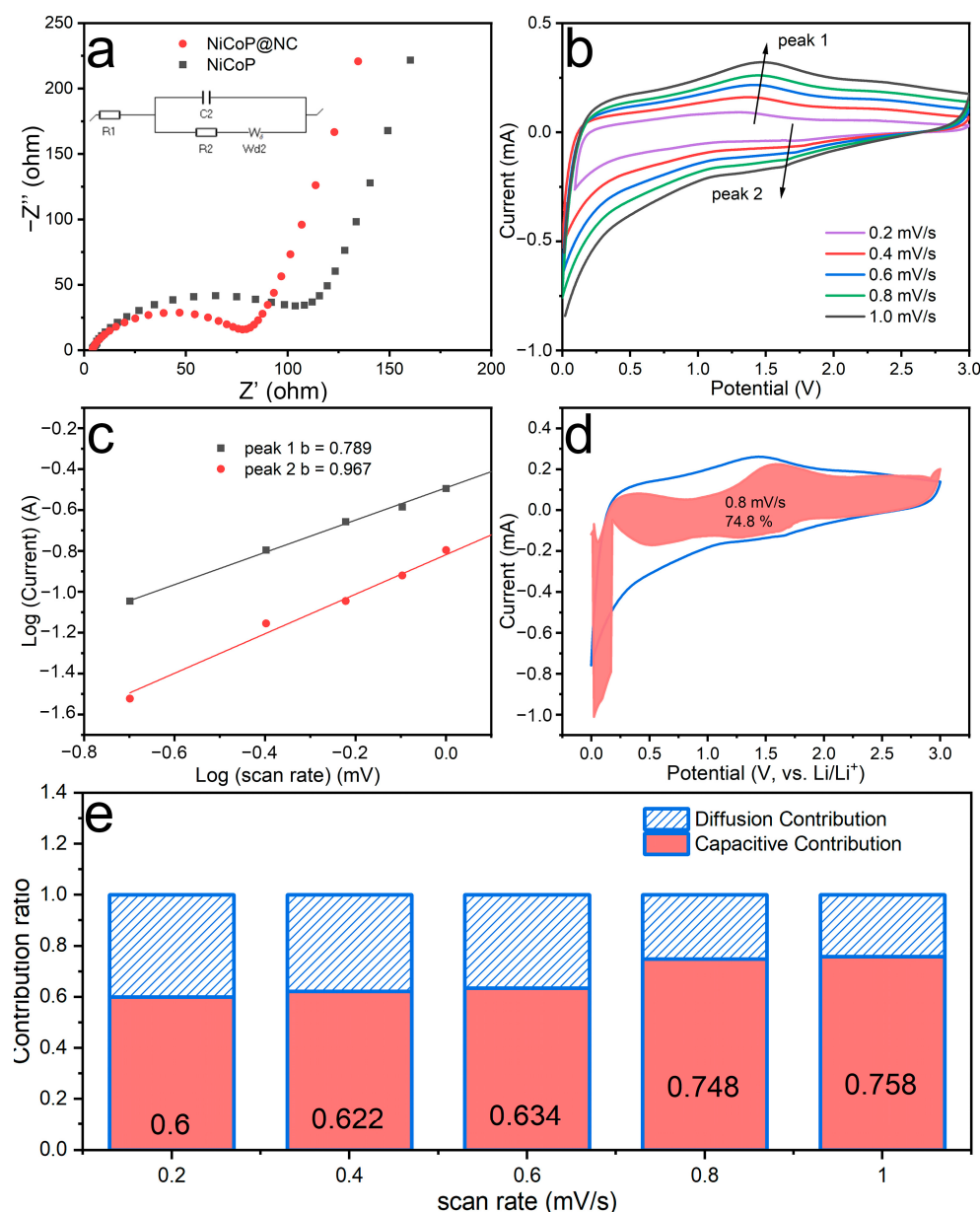


**Figure 6.** (a) EIS of the NiCoP@NC and bare NiCoP cells; (b) Various scan rates (0.2–1 mV/s), CV curves of NiCoP@NC; (c) Related b-value of NiCoP@NC; (d) Capacitive contribution of NiCoP@NC at 0.8 mV/s; (e) Capacitive and diffusion contribution at various scan rates (0.2–1 mV/s).

How the NiCoP@NC electrode possesses the excellent kinetics performance of lithium storage could be attributed to the synergistic effect between flower-like NiCoP (core) and the N-doped carbon (shell) (Figure 7). During the lithium process ( $\text{NiCoP} + 3 \text{ Li}^+ + 3 \text{ e}^- \leftrightarrow \text{Ni} + \text{Co} + \text{Li}_3\text{P}$ ), flower-like NiCoP offers numerous active sites and interfaces that efficiently boost the  $\text{Li}^+$  transfer and establish close contact between electrolyte and electrode. The N-doped carbon shell plays a role in buffering volume expansion during  $\text{Li}^+$  insertion/extraction, preventing the electrode from pulverization and holding the electrode's intactness. In addition, the N-doped carbon shell could assist in the establishment of a long-lasting SEI layer and prevent direct contact between the electrolyte and NiCoP to suppress the erosion of NiCoP by the electrolyte. As a result, the protective N-doped carbon shell significantly enhances structural stability and cycle life [36,37]. Last but not least, the N-doped carbon shell possesses a rapid  $\text{Li}^+$  diffusion channel and excellent electronic conductivity, resulting in an enhanced rate capacity [38,39]. Benefiting from the unique structural design, NiCoP@NC shows improved electrical contact, structural stability, and reaction kinetics, resulting in an enhancement of rate performance, cycling performance, and cycle life.

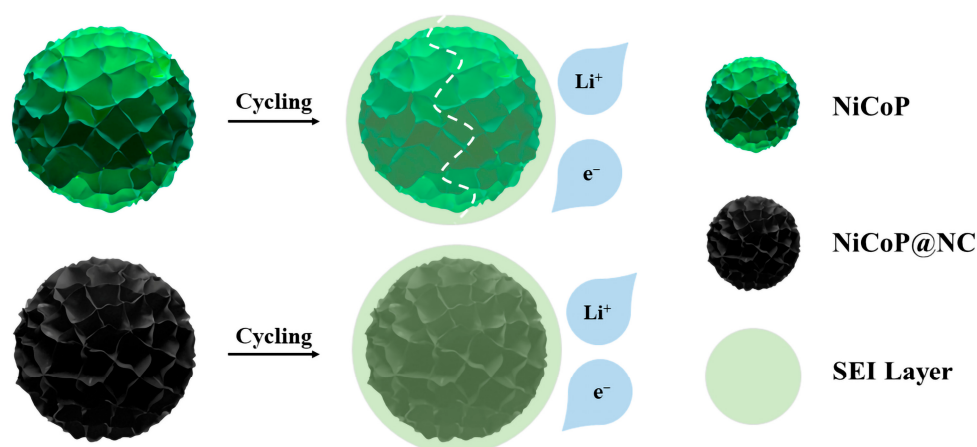


**Figure 7.** Lithiation schematics of bare NiCoP and NiCoP@NC as anode materials for LIBs.

#### 4. Conclusions

To summarize, novel bimetallic flower-like NiCoP encapsulated in an N-doped carbon shell denoted as NiCoP@NC was successfully designed and synthesized as an anode material for LIBs. The flower-like structure of NiCoP offers numerous redox reaction sites and endurance of repeated  $\text{Li}^+$  insertion/extraction processes. The N-doped carbon shell not only enhances the electrical conductivity but also plays a role as a protector to buffer the volume expansion during the  $\text{Li}^+$  insertion/extraction process and prevent direct contact between the electrolyte and NiCoP to avoid the erosion of NiCoP by the electrolyte. NiCoP@NC integrates the advantages of flower-like NiCoP (core) and N-doped carbon (shell) and exhibits a high rate capacity (320.0 mA h/g at 5 A/g), a high specific capacity (545.3 mA h/g at 0.1 A/g with 89% retention), and a long stable cycle life under high current discharge/charge (369.8 mA h/g after 700 cycles at 3 A/g with 81% retention). The kinetics of the electrode process of the NiCoP@NC material was tested using EIS measurement. The results show that the N-doped carbon shell enhances the charge transfer, and the pseudocapacitive behavior dominates the fast  $\text{Li}^+$  storage of the NiCoP@NC anode. The results demonstrate that novel NiCoP@NC can be used as an anode material for high-performance LIBs. This work provides a promising method for developing bimetal phosphides as anode materials for high-performance LIBs.

**Author Contributions:** H.T.: conceptualization and writing. L.Z.: conceptualization and resources. L.W.: supervision and writing. Z.X.: resources. W.T.: resources. Z.J.: supervision and writing. All authors have read and agreed to the published version of the manuscript.

**Funding:** This research was funded by the National Natural Science Foundation of China (Nos: 21601122) and the Belt and Road Initiatives International Cooperation Project (No. 20640770300).

**Data Availability Statement:** Data sharing not applicable.

**Conflicts of Interest:** The authors declare no conflict of interest.

## References

- Wang, X.; Kim, H.-M.; Xiao, Y.; Sun, Y.-K. Nanostructured metal phosphide-based materials for electrochemical energy storage. *J. Mater. Chem. A* **2016**, *4*, 14915–14931. [[CrossRef](#)]
- Hu, C.; Hu, Y.; Chen, A.; Duan, X.; Jiang, H.; Li, C. Atomic Interface Catalytically Synthesizing SnP/CoP Hetero-Nanocrystals within Dual-Carbon Hybrids for Ultrafast Lithium-Ion Batteries. *Engineering* **2022**, *18*, 154–160. [[CrossRef](#)]
- Zhang, Y.; Liu, L.; Zhao, L.; Hou, C.; Huang, M.; Algadi, H.; Li, D.; Xia, Q.; Wang, J.; Zhou, Z.; et al. Sandwich-like CoMoP<sub>2</sub>/MoP heterostructures coupling N, P co-doped carbon nanosheets as advanced anodes for high-performance lithium-ion batteries. *Adv. Compos. Hybrid Mater.* **2022**, *5*, 2601–2610. [[CrossRef](#)]
- Huang, G.; Kong, Q.; Yao, W.; Wang, Q. Poly tannic acid carbon rods as anode materials for high performance lithium and sodium ion batteries. *J. Colloid Interface Sci.* **2023**, *629 Pt A*, 832–845. [[CrossRef](#)]
- Jiang, X.; Chen, Y.; Meng, X.; Cao, W.; Liu, C.; Huang, Q.; Naik, N.; Murugadoss, V.; Huang, M.; Guo, Z. The impact of electrode with carbon materials on safety performance of lithium-ion batteries: A review. *Carbon* **2022**, *191*, 448–470. [[CrossRef](#)]
- Helal, A.; Shaheen Shah, S.; Usman, M.; Khan, M.Y.; Aziz, M.A.; Mizanur Rahman, M. Potential Applications of Nickel-Based Metal-Organic Frameworks and their Derivatives. *Chem. Rec.* **2022**, *22*, e202200055. [[CrossRef](#)]
- Luan, H.; Zhao, A.; Xiao, Y.; Peng, N.; Wen, Y.; Liang, L. Modification of NiCoP nanocages anodes using epoxy-functionalized silane to improve electrochemical performance in lithium-ion batteries. *J. Mater. Sci. Mater. Electron.* **2023**, *34*, 905. [[CrossRef](#)]
- Zhang, Y.; Bo, X.; Nsabimana, A.; Han, C.; Li, M.; Guo, L. Electrocatalytically active cobalt-based metal-organic framework with incorporated macroporous carbon composite for electrochemical applications. *J. Mater. Chem. A* **2015**, *3*, 732–738. [[CrossRef](#)]
- Nayak, P.K.; Yang, L.T.; Brehm, W.; Adelhelm, P. From Lithium-Ion to Sodium-Ion Batteries: Advantages, Challenges, and Surprises. *Angew. Chem. -Int. Ed.* **2018**, *57*, 102–120. [[CrossRef](#)]
- Shang, F.; Yu, W.; Shi, R.; Wan, S.; Zhang, H.; Wang, B.; Cao, R. Enhanced lithium storage performance guided by intricate-cavity hollow cobalt phosphide. *Appl. Surf. Sci.* **2021**, *563*, 150395. [[CrossRef](#)]
- Yang, Y.; Xia, J.; Guan, X.; Wei, Z.; Yu, J.; Zhang, S.; Xing, Y.; Yang, P. In Situ Growth of CoP Nanosheet Arrays on Carbon Cloth as Binder-Free Electrode for High-Performance Flexible Lithium-Ion Batteries. *Small* **2022**, *18*, e2204970. [[CrossRef](#)] [[PubMed](#)]
- Zong, H.; Hu, L.; Wang, Z.; Qi, R.; Yu, K.; Zhu, Z. Metal-organic frameworks-derived CoP anchored on MXene toward an efficient bifunctional electrode with enhanced lithium storage. *Chem. Eng. J.* **2021**, *416*, 129102. [[CrossRef](#)]
- Huang, C.; Ouyang, T.; Zou, Y.; Li, N.; Liu, Z.-Q. Ultrathin NiCo<sub>2</sub>P<sub>x</sub> nanosheets strongly coupled with CNTs as efficient and robust electrocatalysts for overall water splitting. *J. Mater. Chem. A* **2018**, *6*, 7420–7427. [[CrossRef](#)]
- Dang, T.; Wei, D.; Zhang, G.; Wang, L.; Li, Q.; Liu, H.; Cao, Z.; Zhang, G.; Duan, H. Homologous NiCoP/CoP hetero-nanosheets supported on N-doped carbon nanotubes for high-rate hybrid supercapacitors. *Electrochim. Acta* **2020**, *341*, 135988. [[CrossRef](#)]
- Bai, Y.; Zhang, H.; Liu, L.; Xu, H.; Wang, Y. Tunable and Specific Formation of C@NiCoP Peapods with Enhanced HER Activity and Lithium Storage Performance. *Chemistry* **2016**, *22*, 1021–1029. [[CrossRef](#)]
- Wang, J.; Zhu, Y.; Zhang, C.; Kong, F.; Tao, S.; Qian, B.; Jiang, X. Bimetal phosphide Ni<sub>1.4</sub>Co<sub>0.6</sub>P nanoparticle@nitrogen-doped graphene network as high-performance anode materials for lithium-ion batteries. *Appl. Surf. Sci.* **2019**, *485*, 413–422. [[CrossRef](#)]
- Wang, X.-W.; Guo, H.-P.; Liang, J.; Zhang, J.-F.; Zhang, B.; Wang, J.-Z.; Luo, W.-B.; Liu, H.-K.; Dou, S.-X. An Integrated Free-Standing Flexible Electrode with Holey-Structured 2D Bimetallic Phosphide Nanosheets for Sodium-Ion Batteries. *Adv. Funct. Mater.* **2018**, *28*, 1801016. [[CrossRef](#)]
- Zhao, D.Y.; Zhao, R.Z.; Dong, S.H.; Miao, X.G.; Zhang, Z.W.; Wang, C.X.; Yin, L.W. Alkali-induced 3D crinkled porous Ti<sub>3</sub>C<sub>2</sub> MXene architectures coupled with NiCoP bimetallic phosphide nanoparticles as anodes for high-performance sodium-ion batteries. *Energy Environ. Sci.* **2019**, *12*, 2422–2432. [[CrossRef](#)]
- Lu, H.; Qian, R.; Yao, T.; Li, C.; Li, L.; Wang, H. Synthesis of Spherical Carbon-Coated CoP Nanoparticles for High-Performance Lithium-Ion Batteries. *Energy Technol.* **2021**, *9*, 2100605. [[CrossRef](#)]
- Han, L.; Zhang, M.T.; Wang, H.L.; Li, P.; Wei, W.R.; Shi, J.; Huang, M.H.; Shi, Z.C.; Liu, W.; Chen, S.G. Electrospun hetero-CoP/FeP embedded in porous carbon nanofibers: Enhanced Na<sup>+</sup> kinetics and specific capacity. *Nanoscale* **2020**, *12*, 24477–24487. [[CrossRef](#)]
- Shi, S.S.; Sun, C.L.; Yin, X.P.; Shen, L.Y.; Shi, Q.H.; Zhao, K.N.; Zhao, Y.F.; Zhang, J.J. FeP Quantum Dots Confined in Carbon-Nanotube-Grafted P-Doped Carbon Octahedra for High-Rate Sodium Storage and Full-Cell Applications. *Adv. Funct. Mater.* **2020**, *30*, 1909283. [[CrossRef](#)]
- Zheng, H.; Men, S.; Huang, X.L.; Zhou, Y.; Gao, H.C.; Huang, J.; Kang, X.W. Three-dimensional hierarchical Ni<sub>5</sub>P<sub>4</sub> nanospheres encapsulated in graphene as high-performance anode materials of sodium ion batteries. *J. Mater. Sci.* **2020**, *55*, 9027–9036. [[CrossRef](#)]
- Bai, J.; Xi, B.J.; Mao, H.Z.; Lin, Y.; Ma, X.J.; Feng, J.K.; Xiong, S.L. One-Step Construction of N,P-Codoped Porous Carbon Sheets/CoP Hybrids with Enhanced Lithium and Potassium Storage. *Adv. Mater.* **2018**, *30*, 1802310. [[CrossRef](#)]

24. Li, F.F.; Gao, J.F.; He, Z.H.; Kong, L.B. Realizing high-performance and low-cost lithium-ion capacitor by regulating kinetic matching between ternary nickel cobalt phosphate microspheres anode with ultralong-life and super-rate performance and watermelon peel biomass-derived carbon cathode. *J. Colloid Interface Sci.* **2021**, *598*, 283–301. [[CrossRef](#)]
25. Wang, Q.; Hou, M.; Huang, Y.; Li, J.; Zhou, X.; Ma, G.; Ren, S. One-pot synthesis of NiCoP/CNTs composites for lithium ion batteries and hydrogen evolution reaction. *Ionics* **2019**, *26*, 1771–1778. [[CrossRef](#)]
26. Wang, C.; Qian, Y.; Yang, J.; Xing, S.; Ding, X.; Yang, Q. Ternary NiCoP nanoparticles assembled on graphene for high-performance lithium-ion batteries and supercapacitors. *RSC Adv.* **2017**, *7*, 26120–26124. [[CrossRef](#)]
27. Zhu, J.; Yuan, L.; Guan, Q.; Liang, G.; Gu, A. A novel strategy of fabricating high performance UV-resistant aramid fibers with simultaneously improved surface activity, thermal and mechanical properties through building polydopamine and graphene oxide bi-layer coatings. *Chem. Eng. J.* **2017**, *310*, 134–147. [[CrossRef](#)]
28. Guo, H.; Chen, C.; Chen, K.; Cai, H.; Chang, X.; Liu, S.; Li, W.; Wang, Y.; Wang, C. High performance carbon-coated hollow Ni<sub>12</sub>P<sub>5</sub> nanocrystals decorated on GNS as advanced anodes for lithium and sodium storage. *J. Mater. Chem. A* **2017**, *5*, 22316–22324. [[CrossRef](#)]
29. Li, X.; Zhu, X.; Li, J.; Liu, P.; Huang, M.; Xiang, B. Phytic acid-derived Co<sub>2</sub>P/N-doped carbon nanofibers as flexible free-standing anode for high performance lithium/sodium ion batteries. *J. Alloy. Compd.* **2020**, *846*, 156256. [[CrossRef](#)]
30. Guo, H.; Cai, H.; Li, W.; Chen, C.; Chen, K.; Zhang, Y.; Li, Y.; Wang, M.; Wang, Y. Tailored Ni<sub>2</sub>P nanoparticles supported on N-doped carbon as a superior anode material for Li-ion batteries. *Inorg. Chem. Front.* **2019**, *6*, 1881–1889. [[CrossRef](#)]
31. Wang, X.; Chen, K.; Wang, G.; Liu, X.; Wang, H. Rational Design of Three-Dimensional Graphene Encapsulated with Hollow FeP@Carbon Nanocomposite as Outstanding Anode Material for Lithium Ion and Sodium Ion Batteries. *ACS Nano* **2017**, *11*, 11602–11616. [[CrossRef](#)] [[PubMed](#)]
32. Wu, C.; Kopold, P.; van Aken, P.A.; Maier, J.; Yu, Y. High Performance Graphene/Ni<sub>2</sub>P Hybrid Anodes for Lithium and Sodium Storage through 3D Yolk-Shell-Like Nanostructural Design. *Adv. Mater.* **2017**, *29*, 1604015. [[CrossRef](#)] [[PubMed](#)]
33. Zhou, D.; Xue, L.-P.; Wang, N. Robustly immobilized Ni<sub>2</sub>P nanoparticles in porous carbon networks promotes high-performance sodium-ion storage. *J. Alloy. Compd.* **2019**, *776*, 912–918. [[CrossRef](#)]
34. Ren, W.; Zhou, W.; Zhang, H.; Cheng, C. ALD TiO<sub>2</sub>-Coated Flower-like MoS<sub>2</sub> Nanosheets on Carbon Cloth as Sodium Ion Battery Anode with Enhanced Cycling Stability and Rate Capability. *ACS Appl. Mater. Interfaces* **2017**, *9*, 487–495. [[CrossRef](#)]
35. Ge, P.; Zhang, C.; Hou, H.; Wu, B.; Zhou, L.; Li, S.; Wu, T.; Hu, J.; Mai, L.; Ji, X. Anions induced evolution of Co<sub>3</sub>X<sub>4</sub> (X = O, S, Se) as sodium-ion anodes: The influences of electronic structure, morphology, electrochemical property. *Nano Energy* **2018**, *48*, 617–629. [[CrossRef](#)]
36. Yang, Y.; Wang, L.; Zeng, S.; Zhao, K.; Wu, Q.; Yan, L.; Tian, H.; Jiao, Z.; Zhang, J. FeP Coated in Nitrogen/Phosphorus Co-doped Carbon Shell Nanorods Arrays as High-Rate Capable Flexible Anode for K-ion Half/Full Batteries. *J. Colloid Interface Sci.* **2022**, *624*, 670–679. [[CrossRef](#)]
37. Sun, H.; Wang, J.; Li, W.; Yuan, F.; Wang, Q.; Zhang, D.; Wang, B.; Wu, Y.A. Spanish-dagger shaped CoP blooms decorated N-doped carbon branch anode for high-performance lithium and sodium storage. *Electrochim. Acta* **2021**, *388*, 138628. [[CrossRef](#)]
38. Liu, M.; Wang, Q.; Ding, Y.; Jin, Y.; Fang, Z. Co-Salen Complex-Derived CoP Nanoparticles Confined in N-Doped Carbon Microspheres for Stable Sodium Storage. *Inorg. Chem.* **2021**, *60*, 17151–17160. [[CrossRef](#)]
39. Li, H.; Hao, S.; Tian, Z.; Zhao, Z.; Wang, X. Flexible self-supporting Ni<sub>2</sub>P@N-doped carbon anode for superior rate and durable sodium-ion storage. *Electrochim. Acta* **2019**, *321*, 134624. [[CrossRef](#)]

**Disclaimer/Publisher's Note:** The statements, opinions and data contained in all publications are solely those of the individual author(s) and contributor(s) and not of MDPI and/or the editor(s). MDPI and/or the editor(s) disclaim responsibility for any injury to people or property resulting from any ideas, methods, instructions or products referred to in the content.